remote sensing

MDPI

Article

Early Post-Fire Assessments of Wildfires in a Natural Mixed Forest in Northeastern Japan Using Sentinel-2 dNBR and UAV RGB Imagery

Le Tien Nguyen [1], Maximo Larry Lopez Caceres [1,*], Vladislav Bukin [1], Giacomo Corda [1] and Takashi Kunisaki [2]

[1] Faculty of Agriculture, Yamagata University, 1-23 Wakaba-machi, Tsuruoka-shi 997-8555, Japan; u3324003@iwate-u.ac.jp (L.T.N.); u3324009@iwate-u.ac.jp (V.B.)
[2] Faculty of Agriculture, Department of Rural Environmental Sciences, Iwate University, 3-18-8 Ueda, Morioka-shi 020-8550, Japan
* Correspondence: larry@tds1.tr.yamagata-u.ac.jp

Highlights

What are the main findings?

- The 2024 Sentinel-2 dNBR map showed a heterogeneous burn severity pattern, with low and moderate–low severity dominating most plots and higher severity restricted to localized areas.
- UAV RGB interpretation revealed substantial plot-scale variability in tree health condition, with canopy damage being more common than stand-level mortality during the early post-fire stage.

What are the implications of the main findings?

- Sentinel-2 dNBR is effective for landscape-scale mapping of initial burn severity, but it does not fully explain fine-scale variability in tree condition and mortality.
- Integrating UAV imagery with satellite-derived burn severity improves post-fire assessment by providing tree-level health detail in heterogenous forest environments.

Abstract

Unmanned aerial vehicles (UAVs) have become an important component of multi-sensor remote sensing frameworks for post-fire forest monitoring because they provide ultra-high-resolution imagery for evaluating fine-scale vegetation response. This study assessed early-stage post-fire burn severity and forest health condition in a natural mixed forest affected by the 2024 wildfire in Nanyo, Yamagata, northeastern Japan. Burn severity was quantified using the differenced Normalized Burn Ratio (dNBR) derived from Sentinel-2 imagery acquired five months after the fire (October 2024). High-resolution UAV RGB orthomosaics and field surveys were used to classify trees into healthy, damaged, and dead categories. Mean plot-level burn severity was estimated using a weighted midpoint dNBR approach, and the tree mortality rate was calculated from plot-based tree counts. The results showed that low and moderate–low burn severity classes dominated most plots, with mean dNBR values ranging from 0.085 to 0.386. UAV-based interpretation revealed substantial variability in tree health condition among plots. In 2024, fire effects were expressed mainly as canopy damage rather than immediate stand-level mortality. Mortality rates ranged from 14.9% to 58.6%, and some higher-severity plots contained greater damage. Overall, Sentinel-2 dNBR captured landscape-scale burn severity patterns, whereas UAV imagery improved interpretation of fine-scale health variability in heterogeneous burned forests.

Check for updates

Academic Editor: Jungho Im

Received: 28 February 2026
Revised: 14 April 2026
Accepted: 17 April 2026
Published: 22 April 2026

Copyright: © 2026 by the authors. Licensee MDPI, Basel, Switzerland. This article is an open access article distributed under the terms and conditions of the Creative Commons Attribution (CC BY) license.

Keywords: wildfire; satellite; UAV; dNBR; post-fire

1. Introduction

Wildfires represent one of the most significant and frequent disturbances affecting forest ecosystems, with profound ecological, economic and social consequences. In recent decades, the frequency, intensity, and spatial extent of wildfires have escalated globally, driven by complex interactions between climate change, land-use alterations, and anthropogenic activities [1–3]. For land managers, ecologists, and conservationists, the aftermath of large wildfires poses significant challenges since they must precisely estimate damage and forecast recovery paths and put forward practical restoration techniques. Even though traditional field-based monitoring techniques are crucial for detailed ecological insights, they are sometimes limited by logistical constraints, spatial coverage, and temporal frequency—especially in remote, vast, or dangerous post-fire areas. As a result, remote sensing technologies—which provide broad coverage, multi-temporal capabilities, and more complex analytical frameworks—have become crucial tools for thorough post-fire assessment.

Remote sensing techniques have played a central role in post-fire monitoring by enabling large-scale, repeatable assessments of burned areas and burn severity. To monitor the changes in vegetation and soil reflectance caused on by fire, early satellite-based studies relied on Landsat imagery and spectral indices like the Normalized Burn Ratio (NBR) and its temporal differenced counterpart (dNBR) [4,5]. Higher spatial and spectral resolution imagery has enhanced burned area classification and fire severity mapping after the launch of Sentinel-2. To be able to estimate burned areas and classify burn severity for the October 2017 fires in the Iberian Peninsula, ref. [4] developed a Sentinel-2-based methodology that achieved better geographic accuracy than coarser-resolution products like MODIS and operational fire datasets. The effectiveness of Sentinel-2 for burned area detection has also been demonstrated in diverse ecological contexts. For instance, wildfire area detection in Algeria's Beni Salah National Forest highlighted how Sentinel-2 imagery can accurately identify burned areas in humid forest environments, emphasizing its importance for useful fire monitoring in areas with limited data [6]. The advantages of Sentinel-2 over older sensors are further highlighted by comparative studies. Due to its greater spatial resolution and red-edge spectral bands, which increase sensitivity to vegetation condition and post-fire effects, Sentinel-2 has been found to perform better than Landsat 8 in measuring burn severity in Western North America [7].

Despite the strengths of satellite imagery, it is still difficult to identify fine-scale vegetation responses including early post-fire regeneration, species-specific survival, and individual tree mortality. Recent studies have frequently combined satellite observations with unmanned aerial vehicle (UAV) data in order to overcome these limitations. Researchers evaluated vegetation recovery trajectories in Latroon dry forests utilizing Landsat ETM+, UAV imagery, and field surveys. They found that UAV data significantly improves the detection of canopy damage and regrowth patterns that are not visible on the satellite imagery scale [8]. Similarly, multi-source approaches integrating optical, thermal, and UAV datasets have been successfully applied in complex terrain, such as in Chongqing, China, where multi-sensor fusion improved fire mapping accuracy and severity interpretation [9].

The integration of satellite and UAV data represents a promising frontier in post-fire monitoring, potentially leveraging the respective strengths of each platform while mitigating their individual limitation. These integrated methods could allow for complex monitoring frameworks in which UAV data provide fine-scale validation, while satellite

data provide temporal continuity and landscape background. However, there are still technical challenges with cross-platform data fusion, such as uncertainty replication, scale conversion, and geometric and radiometric alignment. Although previous studies [10–13] have demonstrated the potential of UAV data for validating satellite-derived burn severity products, a standardized and transferable framework for UAV–satellite calibration has not yet been established. Moreover, systematic comparisons of burn severity indices derived from both platforms across different fire events and forest types remain limited. This lack of methodological consistency restricts the reliability and broader applicability of multi-scale burn severity assessments.

This study addresses these research gaps by integrating satellite and UAV remote sensing frameworks for early post-fire monitoring in forest ecosystems of northeastern Japan, with two primary objectives: (1) to determine plot-level tree health condition (healthy, damaged, and dead) across burn severity classes using UAV RGB orthomosaic; and (2) to evaluated plot-level tree mortality in relation to mean plot dNBR.

2. Materials and Methods

2.1. Study Area

Akiba mountain is located in southern Yamagata Prefecture (38°4′41.87″N, 140°9′45.95″E) (Figure 1). The maximum elevation is 561 m and the area is dominated mainly by *Pinus densiflora* (Japanese red pine) and *Quercus serrata* (Konara oak).

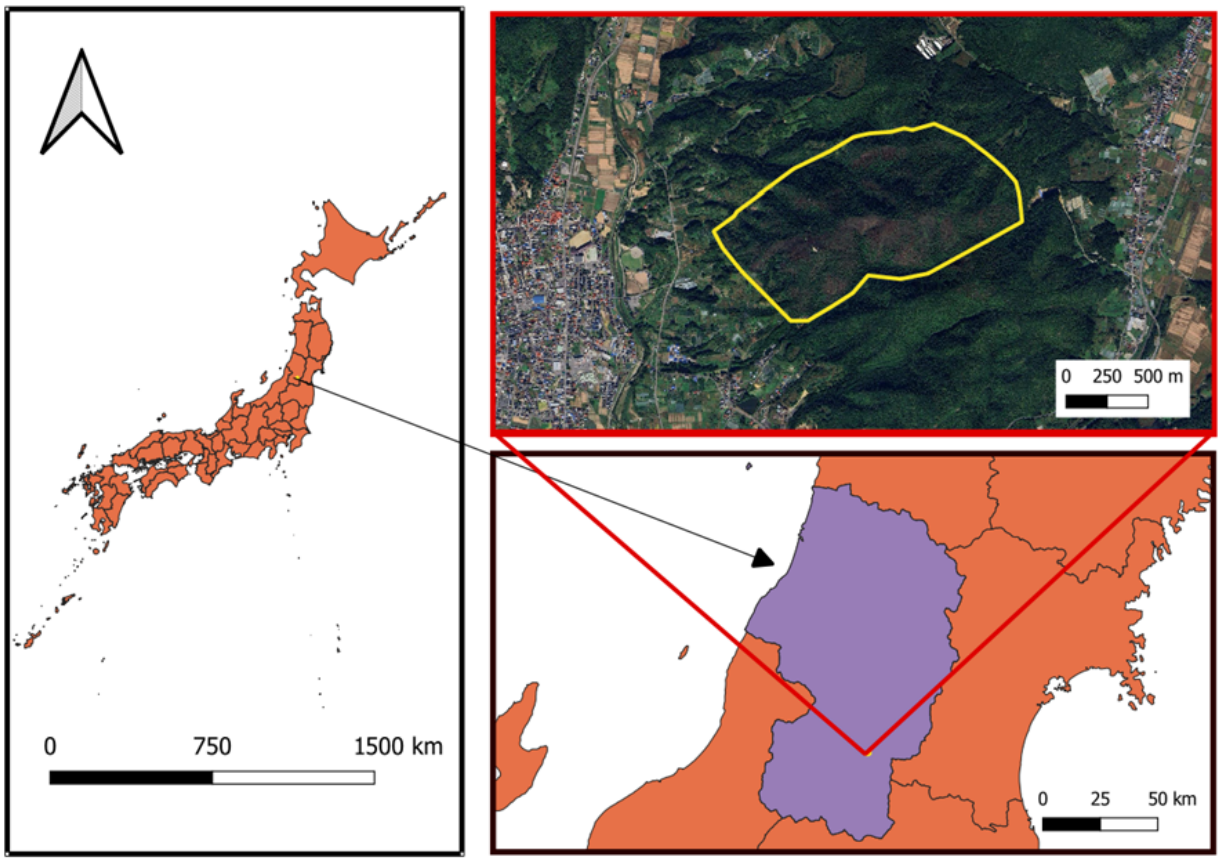

Figure 1. Location of the study area in Nanyo, Yamagata Prefecture, Japan. The map displays the 2024 wildfire perimeter (yellow boundary).

On 4 May 2024, a fire broke out in privately owned forest east of Miyauchi, Nanyo city. According to the official emergency records, the cause remains under investigation; the fire was brought under control on 7 May 2024 and was officially extinguished on

12 May 2024 [14]. The affected area has been reported differently across agencies, with the Forestry Agency listing 102 ha in its wildfire statistics and the FDMA's final report mentions approximately 137 ha [15]. Meteorological conditions likely favored ignition and spread, as the winter of 2023–2024 was characterized by below-normal snowfall in the Sea of Japan coastal area, while AMeDAS observations from Yamagata indicate that April had the lowest mean humidity and the strongest maximum wind speed in the January–April period. These conditions contributed to the prolonged dry conditions that led to fire outbreak [16].

2.2. UAV Image Collection and Pre-Processing

UAV surveys were conducted using a DJI Mavic 3M [17], equipped with one 20 MP 4/3-inch CMOS RGB sensor and four 5 MP multispectral sensors (green, red, red-edge, and near-infrared). The UAV was also equipped with a Real-Time Kinematic (RTK) module, which communicated with a DJI D-RTK 2 GNSS base station to provide centimeter-level positioning accuracy.

The RGB aerial images used in this study were acquired during three surveys: October 2024, May 2025, and October 2025. For each flight, approximately 2367 images were collected. Flight planning was performed in DJI Pilot 2, with a flight altitude of 90 m above ground level, and both frontal and side overlap set to 75%. Each flight lasted less than one hour and was conducted under stable daylight conditions with partial cloud cover.

The collected images were processed in DJI Terra Agriculture Edition v4.2 to generate RGB orthomosaics and digital surface models (DSMs) of the study area (Figure 2). According to the DJI Terra quality report, the reconstruction achieved a georeferencing RMSE of 0.024 m, a reprojection error of 1.14 pixels, and a ground sampling distance (GSD) of approximately 2.88 cm/pixel. The RTK positioning report indicated an average horizontal standard deviation of 1.46 cm and an average vertical standard deviation of 2.47 cm, confirming the high positional accuracy of the UAV products. Although partial cloud cover created shadowing in the images, the orthomosaic generated by DJI Terra used the Light Uniformity function during reconstruction to balance brightness differences between overlapping images and exclude images showing strong shadow artifacts for the final orthomosaic.

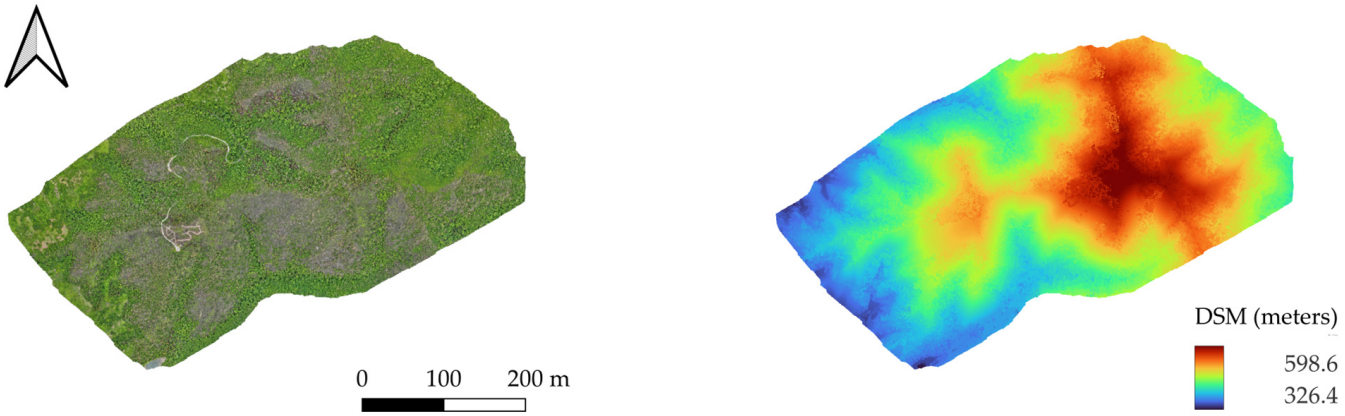

Figure 2. High-resolution UAV photogrammetry products of Nanyo study area, processed using DJI Terra software: (**a**) RGB orthomosaic showing post-fire conditions, and (**b**) digital surface model (DSM) representing the vertical structure of the forest and terrain. The color ramp in panel (**b**) indicates surface elevation in meters above sea level, ranging from dark blue (low elevation, 326.4 m) to dark red (high elevation, 598.6 m).

2.3. Definition of Fire Severity and Burn Severity

The terms fire severity and burn severity are sometimes used interchangeably in wildfire studies, although they describe different processes. Fire severity refers to the immediate physical and chemical effects of combustion during the fire event, including heat release and the consumption of aboveground biomass. In contrast, burn severity refers to the post-fire ecological effects, including changes in vegetation structure, soil condition, and overall ecosystem response.

These two concepts are not always directly equivalent. A fire with high combustion intensity does not necessarily produce the same level of ecological damage across different ecosystems, because post-fire responses depend on vegetation composition, fuel characteristics, and environmental conditions [18]. In remote sensing studies, burn severity is commonly assessed using spectral indices derived from pre- and post-fire satellite imagery. Therefore, in the present study, the term burn severity is used consistently when referring to post-fire effects evaluated from satellite-derived dNBR.

2.4. Satellite Image Collection and Pre-Processing

Sentinel-2 imagery [19] was processed in Google Earth Engine (GEE), a cloud-based platform for large-scale geospatial analysis [20]. GEE enables efficient processing and comparison of pre-fire and post-fire satellite data and has been widely used in environmental and remote sensing studies [21].

Burn severity was quantified using the differenced Normalized Burn Ratio (dNBR). First, the Normalized Burn Ratio (NBR) was calculated from the near-infrared (NIR) and shortwave infrared (SWIR) bands of Sentinel-2:

$$\mathrm{NBR} = \frac{\mathrm{NIR} - \mathrm{SWIR}}{\mathrm{NIR} + \mathrm{SWIR}} \quad (1)$$

The purpose of the differenced Normalized Burn Ratio (dNBR) is to isolate burned from unburned areas and to provide a quantitative measure of change; the NBR post-fire is subtracted from the NBR pre-fire (Equation (2)). The dNBR value indicates the temporal post-fire impact, where positive values correlate with vegetation loss, while negative values usually indicate an increase in vegetation productivity or greenness [22].

In Sentinel-2 imagery, Band 8 represents NIR and Band 12 represents SWIR [23]. NBR is sensitive to fire-related vegetation changes because burned surfaces typically show reduced NIR reflectance and increased SWIR reflectance [22].

The post-fire dNBR was then calculated by subtracting the post-fire NBR from the pre-fire NBR:

$$\mathrm{dNBR} = \mathrm{NBR\ prefire} - \mathrm{NBR\ postfire} \quad (2)$$

Positive dNBR values generally indicate vegetation loss and increased burn impact, whereas negative values indicate increased greenness or vegetation recovery [22].

The processing workflow used in this study was adapted from previous studies [24–26] and modified for the present analysis (Figure 3). The same pre-fire image (April 2024) and post-fire image (October 2024, five months after the wildfire) were used to generate the 2024 dNBR map. In GEE, the SWIR band (Band 12, 20 m resolution) was automatically resampled to match the 10 m resolution of Band 8 during dNBR calculation. The post-fire satellite image and dNBR products were exported using the UAV shapefile extent as the region of interest to ensure consistent spatial extents between the satellite and UAV datasets.

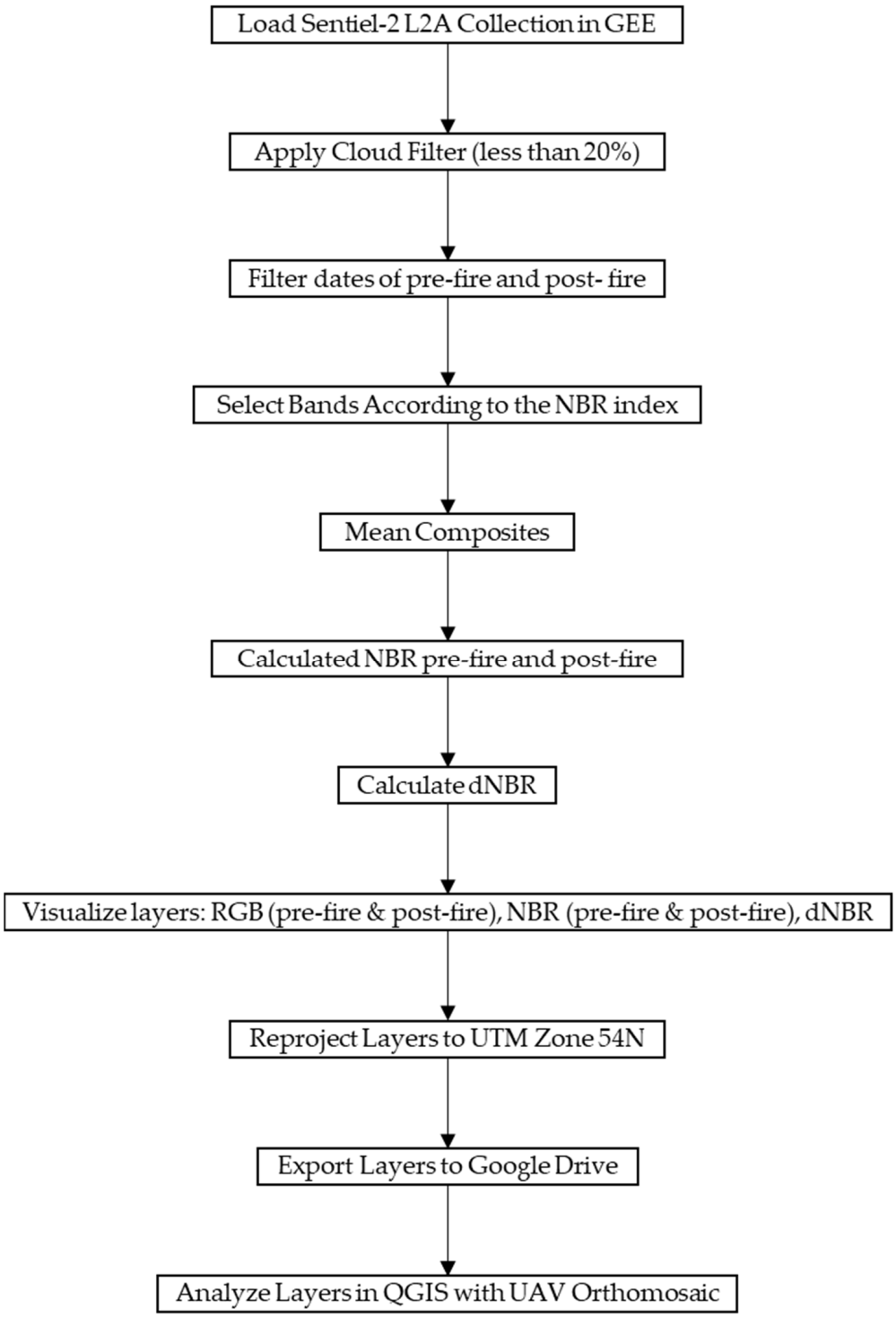

Figure 3. Methodological flowchart of the satellite data processing workflow performed in GEE. The process outlines the acquisition of pre-fire and post-fire Sentinel-2 imagery, the calculation of dNBR, and reproject and export layers for comparison with UAV orthomosaic in QGIS.

2.5. UAV and Satellite Validation

The RGB orthomosaic generated from the first UAV survey in October 2024 was used to establish test plots for initial annotation of tree health condition. During the second UAV campaign in May 2025, a field survey was conducted on the same day as the flight to verify tree-condition interpretation. However, between the 2024 and 2025 surveys, several dead trees near the UAV launch area were mechanically removed. This clear-cutting affected the

consistency of annotation in a small portion of the study area; therefore, the affected area was excluded from further analysis (Figure 4).



Figure 4. Multi-temporal UAV RGB images illustrating a plot excluded from the analysis due to post-fire human-related disturbance. The sequence displays 25 October 2024, showing the initial fire-affected area; 26 May 2025, showing the onset of logging activity; and 23 October 2025, following complete salvage clear-cutting. This plot was removed to ensure the analysis focused strictly on natural fire-induced tree mortality rather than human-driven land-cover changes.

To compare UAV and satellite observations, the UAV orthomosaic and Sentinel-2 imagery was analyzed in QGIS. The UAV orthomosaic was originally referenced in EPSG:4326 (WGS 84), whereas the Sentinel-2 imagery was processed in EPSG:32654 (WGS 84/UTM Zone 54N). To ensure spatial consistency, the UAV orthomosaic was first reprojected to EPSG:32654. Additional spatial refinement was then performed using the Georeferencer tool in QGIS, where five virtual ground control points (GCPs) were manually selected on the UAV orthomosaic and matched to corresponding features on the Sentinel-2 image. After reprojection and refinement, the UAV raster was aligned to the Sentinel-2 grid.

A 10 m × 10 m grid corresponding to the spatial resolution of Sentinel-2 was created over the burned area, and 50 m × 50 m validation plots were established within the study area (Figure 5). Since the Sentinel-2 RGB image is too coarse for individual tree identification, tree-level interpretation was performed using the UAV RGB orthomosaic. The dNBR map was used to assign burn severity classes, and the spatial distribution of healthy, damaged, and dead trees was evaluated within the corresponding burn severity pixels (Table 1).

Table 1. Classification of burn severity levels based on dNBR thresholds, adapted from [27]. The table provides the descriptive severity level, corresponding map color codes, and unscaled dNBR ranges.

Severity Level	Color Code	dNBR Range (Not Scaled)
Enhanced regrowth, high (post-fire)		−0.500 to −0.251
Enhanced regrowth, low (post-fire)		−0.250 to −0.101
Unburned		−0.100 to +0.099
Low severity		+0.100 to +0.269
Moderate–low severity		+0.270 to +0.439
Moderate–high severity		+0.440 to +0.659
High severity		+0.660 to +1.300

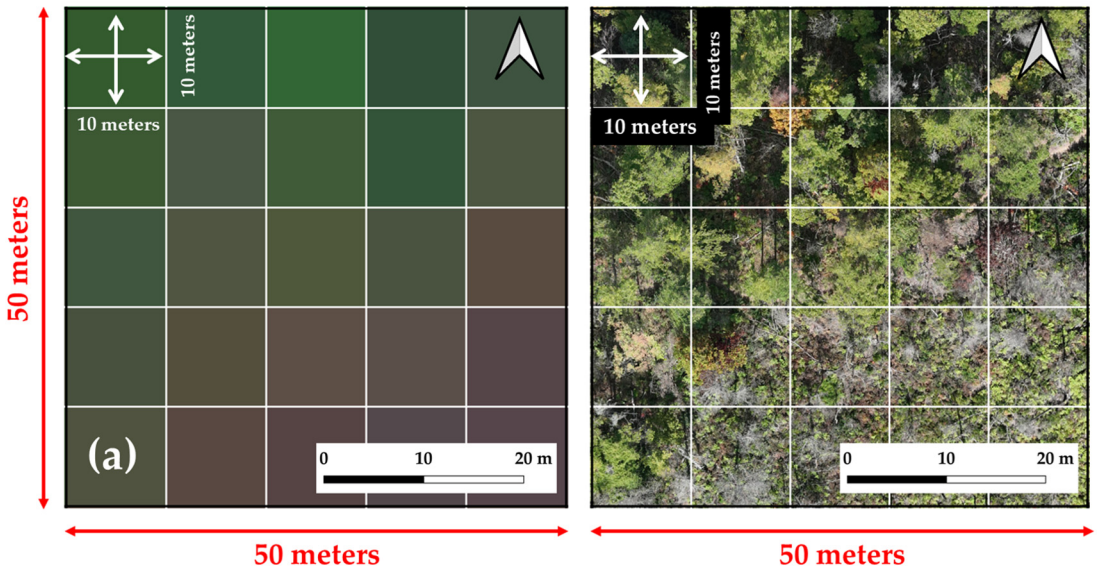

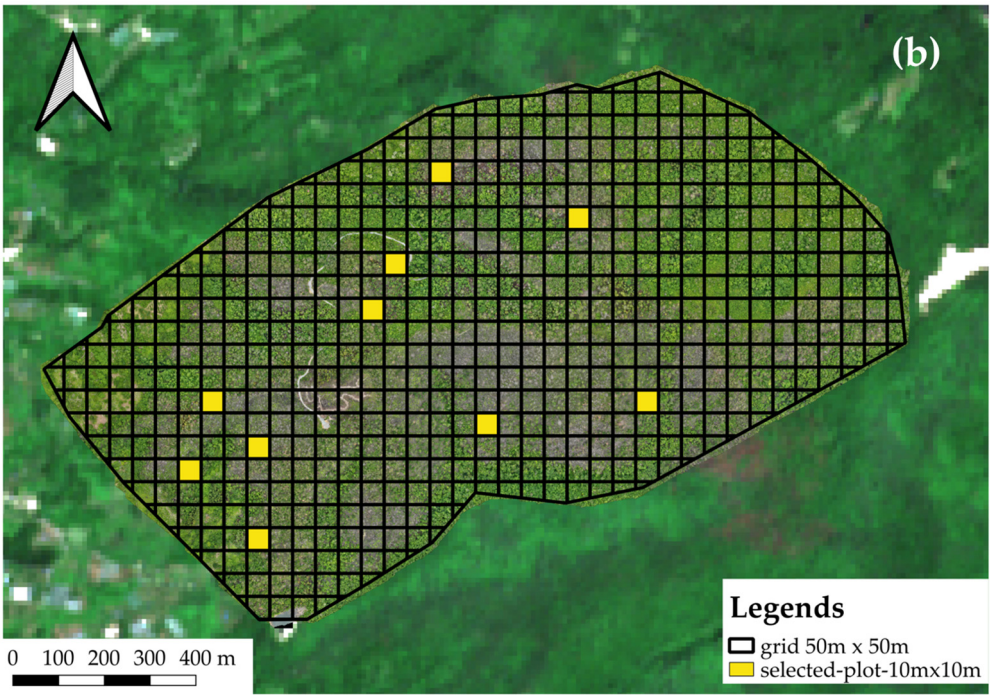

Figure 5. Overview of the multi-scale sampling design and grid alignment between satellite and UAV imagery for the study area: (**a**) Sentinel-2 RGB satellite imagery resampled to a 10 m × 10 m pixel grid; (**b**) corresponding UAV RGB orthomosaic (2 cm/pixel) used to validate the 10 m grid cells; and spatial distribution of the sampling design across the study site, illustrating the 50 m × 50 m references blocks and the 10 selected 10 m × 10 m validation plots (yellow squares).

Plots were selected using a targeted sampling approach based on burn severity. Each 50 m × 50 m plot was required to include at least three of the five burn severity classes: unburned, low, moderate–low, moderate–high, and high severity. The two enhanced regrowth classes were excluded from plot selection because the post-fire period considered in this study was limited to five months, making them less relevant to the initial burn severity assessment. Within each selected plot, the number and distribution of healthy, damaged, and dead trees were recorded for comparison with burn severity patterns.

Although the datasets were orthorectified and co-aligned, minor residual geolocation uncertainty may remain, particularly in Sentinel-2 imagery. Therefore, the comparison was interpreted primarily at the plot scale, rather than as exact pixel-to-crown correspondence for individual trees.

To compare satellite-derived burn severity with plot-level forest condition, each selected 50 m × 50 m plot was subdivided into 25 equal cells corresponding to the spatial framework used for the dNBR overlay. Since individual tree crowns could not be reliably interpreted from Sentinel-2 RGB imagery alone, tree condition was assessed using high-resolution UAV RGB orthomosaics acquired during the post-fire surveys. The resulting spatial comparison was intended to link the burn severity pattern observed in the dNBR layer with visible tree-level health condition within each plot (Figure 6).

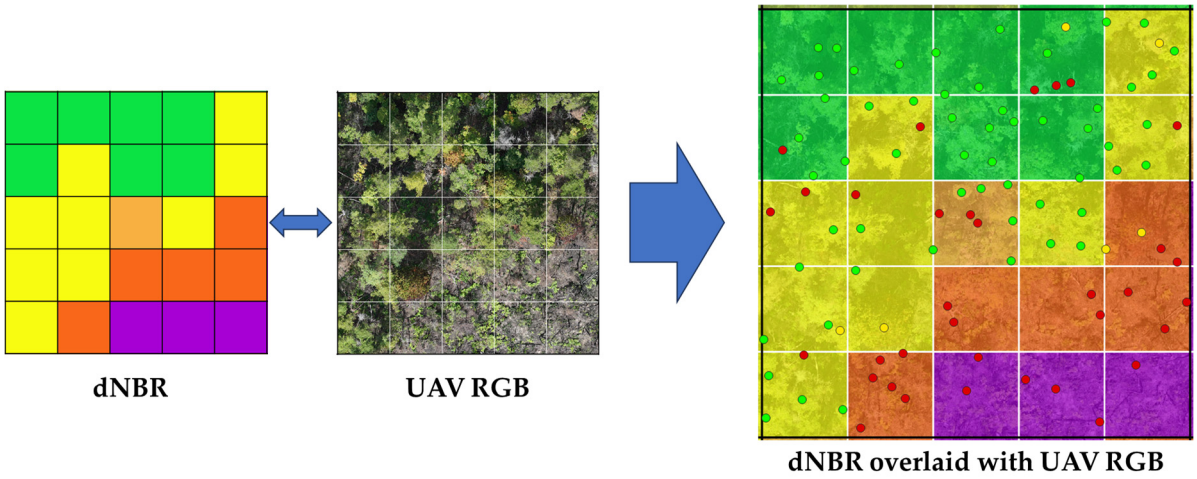

Figure 6. Spatial validation workflow for integrating satellite burn severity with UAV-derived tree distribution: (**Left**) classified Sentinel-2 dNBR pixels representing discrete burn severity levels colors corresponding with Table 1; (**Center**) UAV RGB orthomosaic used for individual tree identification; and (**Right**) the spatial overlay of the dNBR grid on the UAV orthomosaic. Individual tree health status represented by different circle colors: Green (Healthy); Yellow (Damaged); Red (Dead) is visually validated within each 10 m × 10 m dNBR pixel to ensure precise cross-sensor co-registration.

Tree crowns visible in the UAV orthomosaics were visually delineated as polygons and assigned to one of three health condition classes: healthy, damaged, or dead. Healthy trees were identified by crowns retaining predominantly green foliage or needles. Damaged trees were defined as crowns showing partial discoloration, mixed green and brown-red canopy tones, or pale gray to whitish foliage. Dead trees included both standing dead trees with complete defoliation and fallen dead trees recognizable from crown and stem structure in the orthomosaic. These classes represent visible post-fire structural conditions derived from RGB imagery rather than direct physiological measurements of canopy stress (Figure 7).

For each plot, the spatial distribution of annotated tree classes was compared with the dNBR-derived burn severity pattern to examine how the visible canopy condition varied across severity levels. Tree crowns and burn severity cells within a selected plot were overlaid, integrating centimeter-level UAV products with Sentinel-2-derived burn severity classes. The interpretation should be understood as a plot-level spatial comparison dependent on the geospatial alignment of the two datasets, rather than as a direct one-to-one tree-level validation (Figure 8).

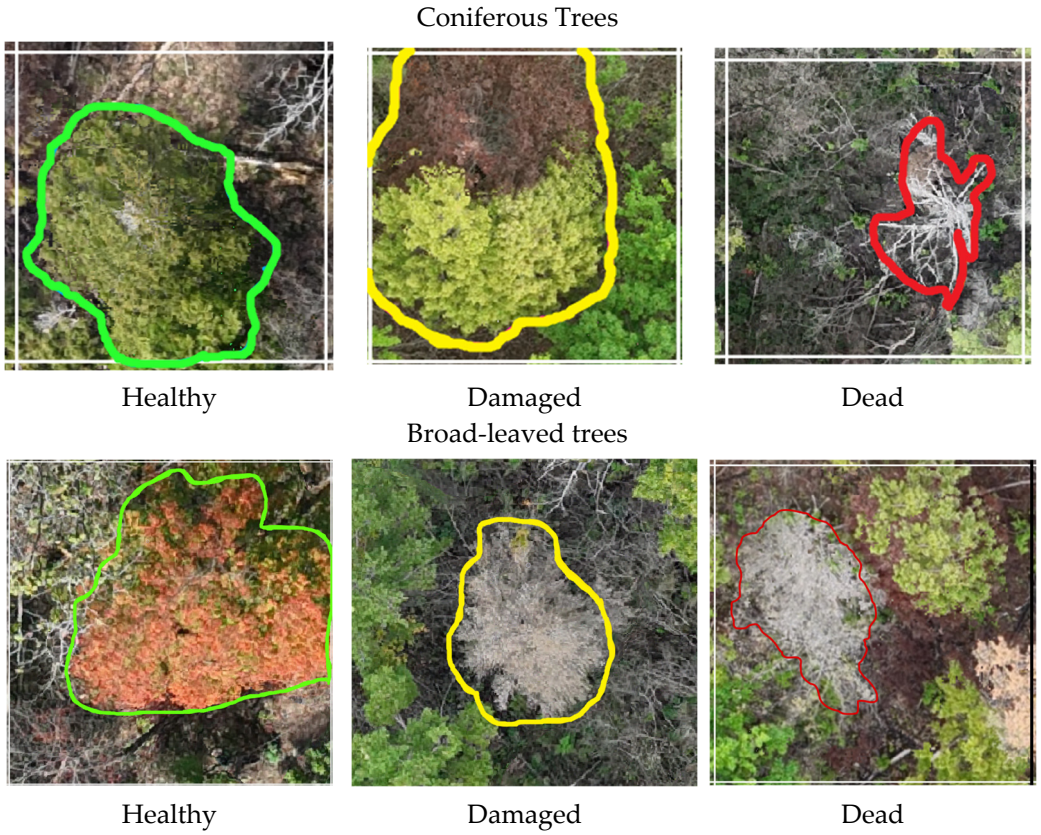

Figure 7. Visual annotation criteria for tree health classification using UAV RGB orthomosaic. The figure illustrates the three classification categories—healthy (green foliage—green polygons), damaged (partial crown scorch or brown needles/leaves—yellow polygons), dead (complete defoliation, gray/white crown structure or visible fallen trees—red polygons)—for both Coniferous and Broad-leaved trees.

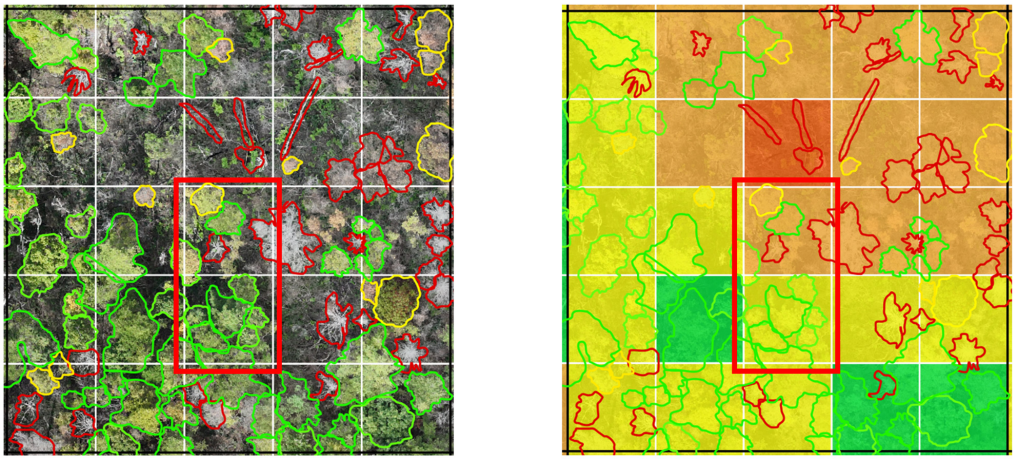

Figure 8. Spatial validation of tree health annotations against dNBR pixels in a representative assessed plot: (**a**) UAV RGB orthomosaic with annotated tree crown polygons, and (**b**) same tree polygons overlaid on the classified dNBR 10 m gird. Polygon outlines represent the tree health classes: green (**healthy**), yellow (**damaged**), and red (**dead**). The rectangular highlights the transition from a "moderate–low severity" (light orange) to "low severity" (yellow), the colors of rectangular in (**b**) is corresponding with Table 1, showing the corresponding increase in surviving healthy crowns (green polygons).

2.6. Mean Burn Severity and Tree Mortality Analysis

To quantitatively assess post-fire disturbance and vegetation response at the plot level, mean burn severity and tree mortality rate were calculated for each validation plot.

Burn severity was represented by mean dNBR. Each field plot measured 50 m × 50 m, corresponding to 25 Sentinel-2 pixels at 10 m spatial resolution. Because raw pixel-level dNBR values were not retained, mean dNBR was estimated using a weighted midpoint approach based on the proportional distribution of burn severity classes within each plot. Representative midpoint values were assigned to each burn severity class (Table 2).

Table 2. Representative midpoint dNBR values calculated for each burn severity level. These midpoints were derived from the standardized dNBR ranges (Table 1) to facilitate quantitative correlation analysis with UAV-derived tree mortality data. The values represent the estimated mean of the upper and lower thresholds for each severity class as defined by the USGS-standardized classification system.

Burn Severity Level	Representative Midpoint dNBR Value
Unburned	0.00
Low severity	0.185
Moderate–low severity	0.355
Moderate–high severity	0.55
High severity	0.80

The mean plot level dNBR is computed as:

$$Mean\ dNBR = \frac{\sum(n_i \times dNBR_i)}{N}$$

where:

- n_i = number of pixels in severity level I;
- $dNBR_i$ = midpoint value of level I;
- N = total number of pixels per plot (25).

Tree mortality was evaluated using tree-condition annotations derived from UAV orthomosaics for the selected plots. Trees were classified into three health categories: healthy, damaged, and dead. The mortality rate was calculated as:

$$Mortality\ Rate\ (\%) = \frac{Dead}{Healthy + Damaged + Dead} \times 100$$

These two metrics were used to compare satellite-derived burn severity with tree-level health response at the plot scale.

To examine the relationship between satellite-derived burn severity and plot-level vegetation response, Spearman's rank correlation coefficient was applied to compare mean dNBR and tree mortality rate across the selected plots. This non-parametric test was chosen because of the small sample size and because it does not require the assumption of a linear relationship between variables.

$$r_s = 1 - \frac{6\sum d_i^2}{N(N^2 - 1)}$$

where:

- d_i is the difference between each pair of ranked variables;
- N is the total number of samples.

3. Results

3.1. Burn Severity Mapping

The selected Sentinel-2 RGB images illustrate the temporal progression of post-fire conditions in the study area from the pre-fire stage (April 2024) to the post-fire observations acquired in October 2024, May 2025, and October 2025 (Figure 9). Compared with the pre-fire image, the post-fire scenes show clear changes in canopy color and surface condition within the burned area. The area affected by subsequent clear-cutting, which was also identified in the UAV orthomosaics, is visible in the later satellite images.

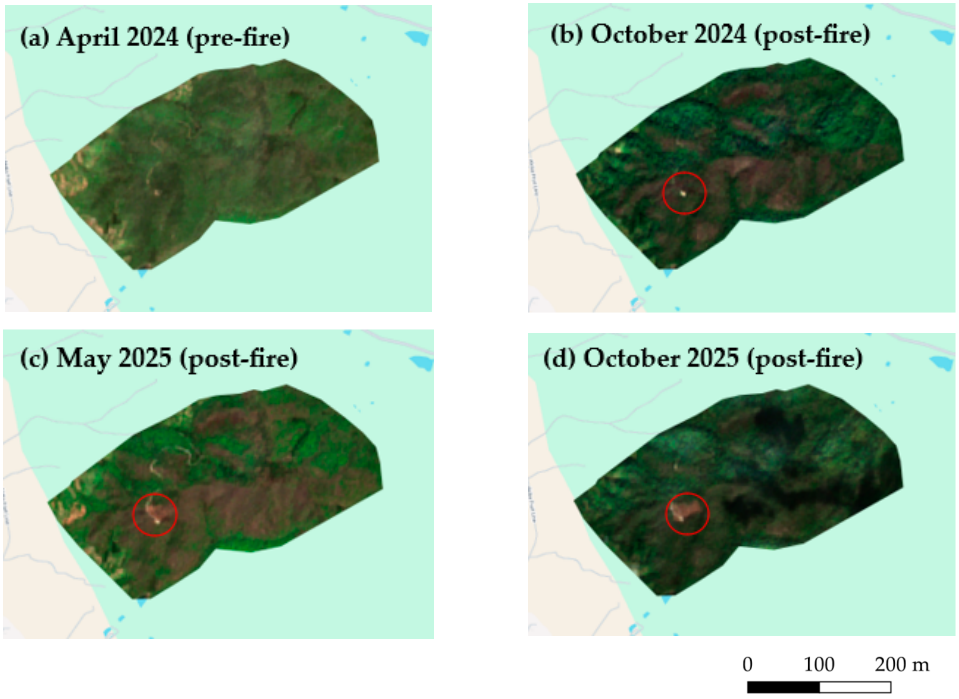

Figure 9. Multi-temporal Sentinel-2 RGB satellite imagery of the study area showing land-cover changes from pre-fire to two years post-fire: (**a**) **April 2024 (pre-fire);** (**b**) **October 2024 (immediate post-fire);** (**c**) **May 2025; and** (**d**) **October 2025**. The red circles highlight an area of human-related disturbance (clear-cutting) that was cross-validated with UAV imagery.

The burn severity map derived from the October 2024 dNBR image revealed a heterogeneous post-fire pattern across the burned forest (Figure 10). Low and moderate–low severity classes occupied most of the study area, indicating that fire effects were largely associated with partial canopy damage and understory burning. Moderate–high and high severity classes were concentrated mainly in the central part of the burned area, forming a continuous belt of stronger fire impact. Unburned patches remained distributed both near the perimeter and within the fire boundary, showing that burn effects were not spatially uniform. Overall, the map indicates that the wildfire produced a mosaic of burn severity levels rather than a consistent stand-replacing disturbance.

At the plot scale, the burn severity classes also showed substantial variability. The selected plots contained mixed severity compositions, with low and moderate–low severity pixels forming the largest proportion in most plots, while moderate–high and high severity pixels occurred in smaller numbers (Figure 11). This confirms that fire effects varied considerably among the sample plots rather than being represented by a single severity class.

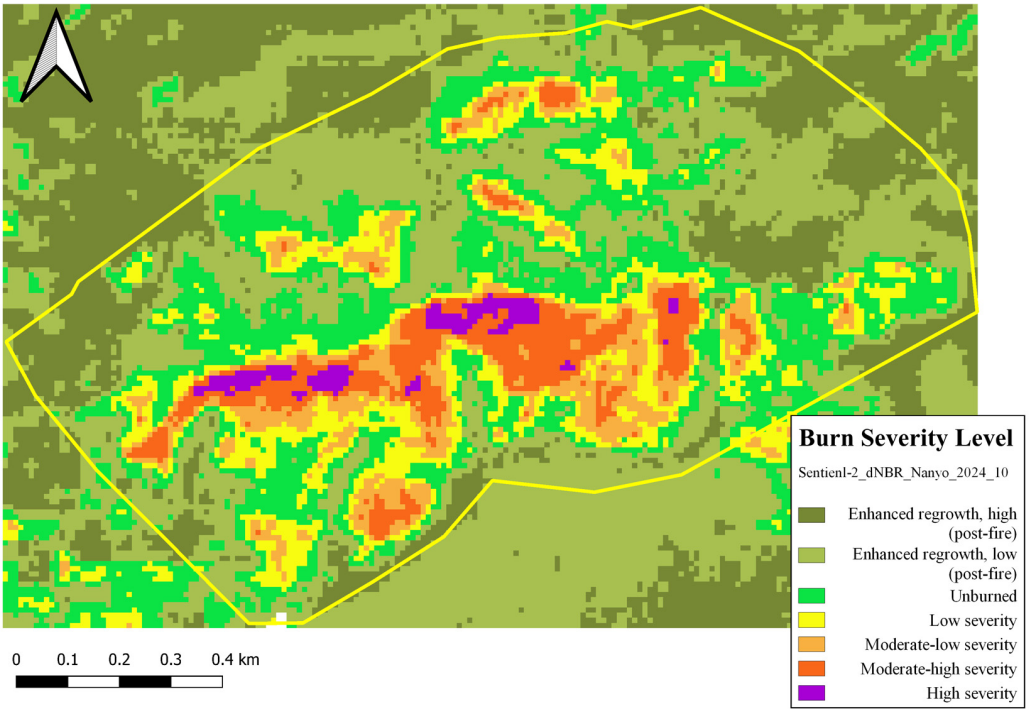

Figure 10. Classified burn severity map of the study area derived from Sentinel-2 dNBR data (October 2024). The map illustrates the spatial distribution of seven severity classes, ranging from "**enhanced regrowth**" to "**high severity**," as defined by the USGS thresholds detailed in Table 1. The yellow boundary indicates the official 2024 wildfire perimeter.

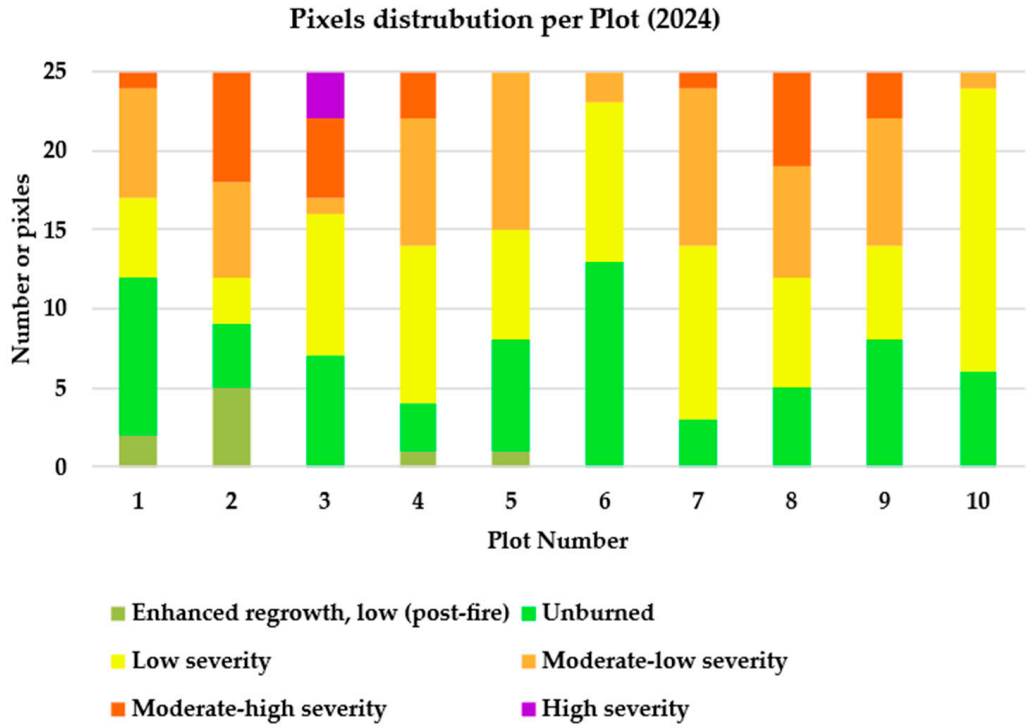

Figure 11. Distribution of Sentinel-2 burn severity pixels within 10 representative plots during the 2024 post-fire season. The stacked bar chart illustrates the frequency (number of 10 m × 10 m pixels) of different dNBR-derived severity classes—ranging from "**enhanced regrowth**" to "**high severity**"—within each plot boundary. This visualization demonstrates the spectral heterogeneity across the study site, which serves as the basis for calculating the mean dNBR values used in subsequent correlation analyses with UAV-derived mortality data.

Mean burn severity values further quantified this variability (Table 3). Mean dNBR ranged from 0.085 to 0.386, with Plot 3 showing the highest value and Plot 6 the lowest. Most plots fell within the low to moderate–low severity range, indicating that the sample areas were primarily affected by low to intermediate levels of burn severity in the immediate post-fire period.

Table 3. Summary of mean dNBR values and corresponding severity interpretations for the 10 plots. The mean dNBR was calculated by averaging all 10 m × 10 m Sentinel-2 pixels within each plot boundary (as visualized in Figure 11). Severity interpretations follow the standardized USGS thresholds adapted for this study (Table 1). These values serve as the independent variable for the Spearman rank correlation analysis against UAV-derived tree mortality.

Plot	Mean dNBR	Severity Interpretation
1	0.316	Moderate–low severity
2	0.297	Moderate–low severity
3	0.386	Moderate–low severity
4	0.264	Low severity
5	0.202	Low severity
6	0.085	Unburned
7	0.245	Low severity
8	0.283	Moderate–low severity
9	0.217	Low severity
10	0.147	Low severity

3.2. Tree Health Condition

The tree health classification results showed clear spatial variability in canopy condition across the selected plots. In the October 2024 orthomosaic, healthy trees were generally more frequent in areas corresponding to unburned and low-burn-severity pixels, whereas damaged and dead trees were more commonly observed in moderate–low- to high-severity areas.

At the plot level, the distribution of tree classes varied substantially among plots (Table 4). The number of healthy trees shows a slight decrease in many plots from 2024 to 2025. Plot 1 declined from 50 to 47 and Plot 3 from 57 to 55, although some plots remained relatively stable, such as Plot 5 (49 to 49). This pattern suggests that while overall stand health remained relatively stable, some delayed mortality may have still occurred. In contrast, damaged trees decreased sharply in almost all plots in 2025; for instance, Plot 5 dropped from 27 damaged trees in 2024 to 0 in 2025. This substantial reduction indicates that previously damaged trees either recovered and were reclassified as healthy or progressed to mortality. Correspondingly, the number of dead trees increased noticeably in many plots in 2025, such as in Plot 5, where dead trees rose from 45 to 72.

The comparison between 2024 and 2025 showed a consistent structural shift in tree condition. Across most plots, the number of damaged trees decreased, while the number of dead trees increased. Healthy tree counts showed relatively smaller changes than the other two classes. This pattern shows that tree health response continued after the initial post-fire observation period.

The spatial distribution of tree classes across burn severity levels further highlights this variability. Healthy trees remained more common in unburned and low-severity pixels, while damaged and dead trees occurred more frequently in the moderate–low, moderate-high, and high severity classes. However, dead trees were also identified in some lower severity pixels, indicating that canopy mortality was not limited to the most severely burned areas.

Table 4. Temporal distribution of tree health classes across the 10 plots, for the 2024 and 2025 growing seasons. Data were derived from individual tree crown segmentation and visual classification using high-resolution UAV RGB imagery. The **healthy, damaged**, and **dead** classes were assigned based on the visual criteria established in Figure 7. These counts provided the basis for calculating the percent tree mortality used to validate the Sentinel-2 dNBR results.

Plot	Healthy		Damaged		Dead	
	2024	2025	2024	2025	2024	2025
1	50	47	0	1	41	43
2	27	25	2	0	41	45
3	57	55	6	0	34	42
4	35	34	13	0	33	47
5	49	49	27	0	45	72
6	75	67	5	4	20	29
7	49	40	15	0	34	58
8	57	51	0	0	10	16
9	53	48	18	3	41	61
10	46	42	22	3	35	58

3.3. Plot-Level Burn Severity and Tree Mortality

Tree mortality rates were calculated for each plot using the proportion of dead trees relative to the total number of healthy, damaged, and dead trees (Table 5). In 2024, mortality ranged from 14.9% to 58.6%, while in 2025 it ranged from 23.9% to 64.3%. Mortality increased between 2024 and 2025 in all plots, although the magnitude of increase differed among plots.

Table 5. Annual cumulative tree mortality rates (%) across 10 plots, for the 2024 and 2025 growing seasons. Mortality percentages were calculated as the ratio of "dead" trees to the total number of trees identified within each 10 m × 10 m plot using high-resolution UAV RGB imagery (based on the raw counts provided in Table 4).

Plot	Mortality 2024	Mortality 2025
1	45.1%	47.3%
2	58.6%	64.3%
3	35.1%	43.3%
4	40.7%	58.0%
5	37.2%	59.5%
6	20.0%	29.0%
7	34.7%	59.2%
8	14.9%	23.9%
9	36.6%	54.5%
10	34.0%	56.3%

A descriptive comparison of mean dNBR and mortality rate showed that some plots with higher burn severity also contained larger proportions of damaged and dead trees. However, this pattern was not consistent across all plots. Some low-severity plots also showed substantial mortality, particularly in 2025. Therefore, although mean dNBR captured plot-level variation in burn severity, the mortality response varied considerably among plots.

Tables 6 and 7 represent the ranked values of mean dNBR and plot-level mortality used for Spearman's rank correlation analysis. Table 6 ranks the ten plots according to mean dNBR, from the lowest burn severity (Plot 6) to the highest (Plot 3). Table 7 ranks plot-level mortality in 2024 and 2025. Comparison of these rank orders showed that the monotonic relationship between burn severity and mortality was weak. In 2024, the rank

correlation indicated a moderated positive but non-significant relationship between mean dNBR and mortality rate (r_s = 0.442, p_{value} = 0.200). In 2025, this relationship was near zero and non-significant (r_s = −0.079, p_{value} = 0.829). These results indicate that, although sone higher severity plots showed greater mortality, the rank order of mortality was not consistently aligned with the burn severity gradient across the ten plots.

Table 6. Ranking of the 10 plots, based on mean dNBR values (as calculated in Table 3). This total ranking (1 to 10) serves as the primary input for the Spearman rank correlation analysis, comparing satellite-derived fire severity against the UAV-derived tree mortality rates for 2024 and 2025.

Plot	dNBR	Rank
6	0.085	1
10	0.147	2
5	0.202	3
9	0.217	4
7	0.245	5
4	0.264	6
8	0.283	7
2	0.297	8
1	0.316	9
3	0.386	10

Table 7. Summary of annual tree mortality rates and corresponding ordinal ranks for the 10 monitoring plots. Mortality percentages represent the proportion of "dead" trees relative to total stems per 10 m × 10 m plot, derived from UAV RGB imagery. Ranks are assigned from 1 (lowest mortality) to 10 (highest mortality) for both 2024 and 2025. These ranks are compared against the dNBR ranks (Table 6) to determine the Spearman correlation coefficient r_s.

Plot	Mortality 2024	Rank 2024	Mortality 2025	Rank 2025
1	45.1%	9	47.3%	4
2	58.6%	10	64.3%	10
3	35.1%	5	43.3%	3
4	40.7%	8	58.0%	7
5	37.2%	7	59.5%	8
6	20.0%	2	29.0%	2
7	34.7%	4	59.2%	9
8	14.9%	1	23.9%	1
9	36.6%	6	54.5%	5
10	34.0%	3	56.3%	6

4. Discussion

4.1. Burn Severity Pattern and Tree Health Response

The 2024 dNBR map revealed a heterogeneous burn severity pattern across the study area, with low and moderate–low severity classes dominating most plots and higher severity concentrated in localized patches. This spatial pattern was consistent with the UAV-based tree interpretation, which showed substantial variation in canopy condition among plots. In general, healthy trees were more common in unburned and low-severity pixels, whereas damaged and dead trees were more frequently observed in moderate–low to high severity classes. However, dead trees were also identified in some lower severity pixels, indicating that mortality was not restricted to the most severely burned areas. These results suggest that the 2024 dNBR map captured broad spatial variability in burn severity, but that the plot-level tree response remained heterogeneous.

The tree-class distribution further showed that post-fire effects were initially expressed more as visible canopy damage than as immediate stand-level mortality. In 2024, damaged trees constituted a substantial fraction of the tree population in several plots, while dead trees were already present across the burned area. By 2025, the number of damaged trees decreased markedly and the number of dead trees increased in most plots, indicating a continued health shift after the first post-fire assessment. This pattern is consistent with delayed mortality processes reported in post-fire forest studies, where trees that survived the fire event may subsequently decline due to physiological stress, cambial injury, or secondary damage. At the same time, the present study only covers the first two years after the fire, and therefore the observed changes should be interpreted as early-stage post-fire structural response rather than long-term forest recovery.

Although some plots with relatively higher mean dNBR values contained greater proportions of damaged and dead trees, the relationship between mean dNBR and mortality rate was not consistent across all plots. In particular, the Spearman analysis did not detect a statistically significant monotonic relationship between mean dNBR and mortality in 2024 or 2025. These results suggest that burn severity alone did not fully explain the variation in plot-level mortality. Local factors such as canopy composition, microsite conditions, mixed-pixel effects, and post-fire stress likely contributed to the variability in tree response. Therefore, the dNBR map should be interpreted as a useful representation of landscape-scale burn severity, rather than as a direct predictor of tree mortality in every plot.

4.2. Integration of UAV and Satellite for Post-Fire Assessment

The integration of UAV imagery and satellite-derived burn severity metrics remains one of the main strengths of this study. Sentinel-2 dNBR provided efficient spatial coverage for mapping post-fire conditions across the entire burned area, while the UAV RGB orthomosaics provided ultra-high-resolution information on tree structural condition at the crown scale. This combination allowed burn severity to be interpreted not only as a spectral response, but also in relation to visible canopy damage and mortality patterns.

However, the comparison between these two datasets also highlights the challenges of linking satellite-derived burn severity to tree-level structural outcomes. A 10 m Sentinel-2 pixel can contain a mixture of healthy trees, damaged trees, dead trees, canopy shadows, exposed soil, and understory vegetation. As a result, the spectral signal represented by dNBR is an average response at the pixel level and may not correspond directly to the structural condition of every tree within that pixel. This helps explain why dead trees were observed in some pixels classified as low severity and why mean dNBR did not show a significant monotonic relationship with mortality across all plots.

Previous studies have similarly emphasized that UAV data improve the interpretation of satellite-derived burn severity products by revealing fine-scale variability that is not detectable at moderate resolutions [10–12]. The present study supports that perspective. In this case, UAV RGB imagery was especially useful for identifying structural classes of healthy, damaged, and dead trees and for illustrating the patchiness of the post-fire canopy condition. Thus, the UAV data did not replace the satellite-derived burn severity map, but rather provided a finer-scale structural context for interpreting it.

At the same time, this study also shows that a multi-scale approach must be applied carefully. Although the UAV orthomosaics were orthorectified, RTK-supported, and further refined through reprojection and co-registration, minor spatial uncertainty may still remain between the UAV and Sentinel-2 datasets. For this reason, the comparison is most reliable at the plot scale, using aggregated metrics such as mean dNBR and tree mortality rate, rather than exact pixel-to-crown correspondence for every tree.

4.3. Limitations and Implications for Future Research

Several limitations of the present study should be acknowledged. First, the assessment of tree condition was based on manual visual interpretation of RGB orthomosaics, supported by field observations, rather than on automated classification or multispectral stress indicators. This approach was appropriate for identifying major structural categories such as healthy, damaged, and dead trees, but it may not capture subtle physiological stress or early sub-lethal canopy decline. In addition, the study methodology was adapted from studies by [28,29], who characterized tree health based on expert annotations of UAV RGB images. Since the area in question is 100 ha, it is physically impossible to validate all trees in the field, and for that reason only a small number were selected for validation. The absence of UAV multispectral analysis therefore limits the ability to evaluate pre-mortality stress responses.

Second, the quantitative validation of UAV-based tree classification was constrained by field accessibility. Only one plot could be verified directly in the field due to steep terrain and difficult post-fire conditions. As a result, classification agreement with field observations was limited and should be interpreted cautiously. Future work should incorporate more systematic field sampling, formal accuracy assessment, and, where possible, automated or semi-automated tree classification procedures.

Third, the present analysis did not include detailed stand structural variables or soil properties, which may also influence burn severity and post-fire mortality. In addition, the monitoring period was limited to the first and second post-fire years. Because forest recovery often extends over much longer periods, the present findings should be regarded as representing initial post-fire structural dynamics rather than full regeneration trajectories.

Despite these limitations, this study demonstrates that combining satellite-derived burn severity mapping with UAV-based structural interpretation provides a useful framework for early post-fire monitoring in heterogeneous forest environments. The results indicate that dNBR is effective for identifying broad burn severity patterns, while UAV imagery provides important detail on tree-level structural response that cannot be captured by satellite data alone. Future studies integrating UAV multispectral indices, longer-term monitoring, and more robust validation approaches would further strengthen this multi-scale framework for post-fire forest assessment.

5. Conclusions

This study evaluated early post-fire forest structural response in a natural mixed forest in Nanyo, Yamagata, northeastern Japan, by integrating Sentinel-2-derived dNBR, UAV RGB orthomosaics, and field observations. The 2024 dNBR map revealed a heterogeneous burn severity pattern, with low and moderate–low severity dominating most plots and higher severity restricted to localized areas.

At the plot scale, UAV-based interpretation showed that post-fire effects were expressed mainly as canopy damage rather than immediate stand-level mortality. Damaged trees were abundant in 2024, whereas dead trees increased by 2025, indicating continued structural change during the first two post-fire years. Mortality rates varied substantially among plots, showing that tree response was spatially heterogeneous.

Although some higher-severity plots contained greater damage, the relationship between mean dNBR and plot-level mortality was not consistent across all plots. This indicates that satellite-derived burn severity effectively represents broad spatial variation in fire effects, but does not fully explain local mortality patterns.

Overall, the results demonstrate that combining satellite-based burn severity mapping with UAV-based tree-level interpretation provides an effective framework for early post-fire assessment in heterogeneous forest environments. Finally, since this study covers only

the first two post-fire years, the findings should be interpreted as initial post-fire structural dynamics rather than long-term forest recovery. Future work should include longer monitoring periods, multispectral UAV analysis, and more systematic field validation.

Author Contributions: Conceptualization: L.T.N.; Methodology: L.T.N.; Software: L.T.N. and V.B.; Validation: L.T.N. and M.L.L.C.; Formal analysis: L.T.N.; Investigation: L.T.N., V.B. and G.C.; Resources: L.T.N. and G.C.; Data curation: L.T.N.; Writing—original draft: L.T.N.; Writing—review and editing: L.T.N. and M.L.L.C.; Visualization: L.T.N.; Supervision: M.L.L.C. and T.K. All authors have read and agreed to the published version of the manuscript.

Funding: This research received no external funding.

Data Availability Statement: Dataset available on request from the authors.

Acknowledgments: We gratefully acknowledge the support provided by the members of the Smart Forest Laboratory for data collection, validation during fieldwork surveys, and software processes. Their contributions were crucial to this research. We also extend our thanks to the anonymous reviewers for their insightful comments and suggestions, which greatly enhanced the quality of this manuscript.

Conflicts of Interest: The authors declare no conflicts of interest.

Abbreviations

UAV	Unmanned Aerial Vehicle
NBR	Normalized Burn Ratio
NIR	Near-infrared
SWIR	Shortwave Near-infrared
AMeDAS	Automated Meteorological Data Acquisition System
RTK	Real-Time Kinematic
GNSS	Global Navigational Satellite System
GEE	Google Earth Engine

References

1. Bowman, D.M.J.S.; Balch, J.K.; Artaxo, P.; Bond, W.J.; Carlson, J.M.; Cochrane, M.A.; D'Antonio, C.M.; DeFries, R.S.; Doyle, J.C.; Harrison, S.P.; et al. Fire in the Earth System. *Science* **2009**, *324*, 481–484. [CrossRef]
2. Chu, T.; Guo, X. Remote Sensing Techniques in Monitoring Post-Fire Effects and Patterns of Forest Recovery in Boreal Forest Regions: A Review. *Remote Sens.* **2013**, *6*, 470–520. [CrossRef]
3. Crowley, M.A.; Stockdale, C.A.; Johnston, J.M.; Wulder, M.A.; Liu, T.; McCarty, J.L.; Rieb, J.T.; Cardille, J.A.; White, J.C. Towards a Whole-system Framework for Wildfire Monitoring Using Earth Observations. *Glob. Change Biol.* **2023**, *29*, 1423–1436. [CrossRef]
4. Llorens, R.; Sobrino, J.A.; Fernández, C.; Fernández-Alonso, J.M.; Vega, J.A. A Methodology to Estimate Forest Fires Burned Areas and Burn Severity Degrees Using Sentinel-2 Data. Application to the October 2017 Fires in the Iberian Peninsula. *Int. J. Appl. Earth Obs. Geoinf.* **2021**, *95*, 102243. [CrossRef]
5. Han, A.; Qing, S.; Bao, Y.; Na, L.; Bao, Y.; Liu, X.; Zhang, J.; Wang, C. Short-Term Effects of Fire Severity on Vegetation Based on Sentinel-2 Satellite Data. *Sustainability* **2021**, *13*, 432. [CrossRef]
6. Zennir, R.; Khallef, B. Forest Fire Area Detection Using Sentinel-2 Data: Case of the Beni Salah National Forest—Algeria. *J. For. Sci.* **2023**, *69*, 33–40. [CrossRef]
7. Howe, A.A.; Parks, S.A.; Harvey, B.J.; Saberi, S.J.; Lutz, J.A.; Yocom, L.L. Comparing Sentinel-2 and Landsat 8 for Burn Severity Mapping in Western North America. *Remote Sens.* **2022**, *14*, 5249. [CrossRef]
8. Qarallah, B.; Al-Ajlouni, M.; Al-Awasi, A.; Alkarmy, M.; Al-Qudah, E.; Naser, A.B.; Al-Assaf, A.; Gevaert, C.M.; Al Asmar, Y.; Belgiu, M.; et al. Evaluating Post-Fire Recovery of Latroon Dry Forest Using Landsat ETM+, Unmanned Aerial Vehicle and Field Survey Data. *J. Arid Environ.* **2021**, *193*, 104587. [CrossRef]
9. Zhao, Y.; Huang, Y.; Sun, X.; Dong, G.; Li, Y.; Ma, M. Forest Fire Mapping Using Multi-Source Remote Sensing Data: A Case Study in Chongqing. *Remote Sens.* **2023**, *15*, 2323. [CrossRef]
10. Fraser, R.; Van Der Sluijs, J.; Hall, R. Calibrating Satellite-Based Indices of Burn Severity from UAV-Derived Metrics of a Burned Boreal Forest in NWT, Canada. *Remote Sens.* **2017**, *9*, 279. [CrossRef]

11. Carvajal-Ramírez, F.; Marques Da Silva, J.R.; Agüera-Vega, F.; Martínez-Carricondo, P.; Serrano, J.; Moral, F.J. Evaluation of Fire Severity Indices Based on Pre- and Post-Fire Multispectral Imagery Sensed from UAV. *Remote Sens.* **2019**, *11*, 993. [CrossRef]
12. Pádua, L.; Guimarães, N.; Adão, T.; Sousa, A.; Peres, E.; Sousa, J.J. Effectiveness of Sentinel-2 in Multi-Temporal Post-Fire Monitoring When Compared with UAV Imagery. *ISPRS Int. J. Geo-Inf.* **2020**, *9*, 225. [CrossRef]
13. Gao, B.; Jia, W.; Wang, Q.; Yang, G. All-Weather Forest Fire Automatic Monitoring and Early Warning Application Based on Multi-Source Remote Sensing Data: Case Study of Yunnan. *Fire* **2025**, *8*, 344. [CrossRef]
14. Special Disaster Office, Fire and Disaster Management Agency. *Damage Caused by Forest Fire in Nanyo City, Yamagata Prefecture and Response by Firefighting Agencies (5th Report)*; Special Disaster Office, Fire and Disaster Management Agency: Tokyo, Japan, 2024.
15. Ministry of Agriculture, Forestry and Fisheries. *Forest Fire Information*; Ministry of Agriculture, Forestry and Fisheries: Tokyo, Japan, 2024.
16. JMA. *Monthly Meteorological Data for Yamagata, Yamagata Prefecture*; JMA: Tokyo, Japan, 2024.
17. DJI. *DJI Mavic 3M*; DJI: Shenzhen, China, 2024.
18. Keeley, J.E. Fire Intensity, Fire Severity and Burn Severity: A Brief Review and Suggested Usage. *Int. J. Wildland Fire* **2009**, *18*, 116–126. [CrossRef]
19. ESA. *Sentinel-2 Mission*; ESA: Paris, France, 2015.
20. Gorelick, N.; Hancher, M.; Dixon, M.; Ilyushchenko, S.; Thau, D.; Moore, R. Google Earth Engine: Planetary-Scale Geospatial Analysis for Everyone. *Remote Sens. Environ.* **2017**, *202*, 18–27. [CrossRef]
21. Kumar, L.; Mutanga, O. Google Earth Engine Applications Since Inception: Usage, Trends, and Potential. *Remote Sens.* **2018**, *10*, 1509. [CrossRef]
22. Key, C.H.; Benson, N.C. *Landscape Assessment (LA)*; USDA Forest Service: Fort Collins, CO, USA, 2006.
23. Sinergise. *Sentinel-2 L2A-Sentinel Hub API Documentation*; Sinergise: Ljubljana, Slovenia, 2024.
24. Xulu, S.; Mbatha, N.; Peerbhay, K. Burned Area Mapping over the Southern Cape Forestry Region, South Africa Using Sentinel Data within GEE Cloud Platform. *ISPRS Int. J. Geo-Inf.* **2021**, *10*, 511. [CrossRef]
25. Gülci, S.; Wing, M.G. Evaluating Forest Fire Severity and Vegetative Recovery Using Sentinel Imagery and Spectral Indices in a Cloud-Based Environment. *Adv. Space Res.* **2025**, *76*, 4092–4105. [CrossRef]
26. Şerifoğlu Yılmaz, Ç. Assessment of Burned Area and Fire Severity Using Sentinel-2 Imagery: Case Studies from Türkiye's Summer 2025 Wildfires. *Turk. J. Remote Sens. GIS* **2025**, *6*, 300–314. [CrossRef]
27. UNOOSA. Detail: Normalized Burn Ratio. In *Recommended Practice: Burn Severity Mapping*; UNOOSA: Vienna, Austria, 2021.
28. Tran, T.C.N.; Caceres, M.L.L.; Riera, S.G.I.; Conciatori, M.; Kuwabara, Y.; Tsou, C.-Y.; Diez, Y. Using UAV RGB Images for Assessing Tree Species Diversity in Elevation Gradient of Zao Mountains. *Remote Sens.* **2024**, *16*, 3831. [CrossRef]
29. Leidemer, T.; Caceres, M.L.L.; Diez, Y.; Ferracini, C.; Tsou, C.-Y.; Katahira, M. Evaluation of Temporal Trends in Forest Health Status Using Precise Remote Sensing. *Drones* **2025**, *9*, 337. [CrossRef]

Disclaimer/Publisher's Note: The statements, opinions and data contained in all publications are solely those of the individual author(s) and contributor(s) and not of MDPI and/or the editor(s). MDPI and/or the editor(s) disclaim responsibility for any injury to people or property resulting from any ideas, methods, instructions or products referred to in the content.